Thermoelectric performance of single phase p-type quaternary (PbTe)0.65–x(PbSe)0.35(PbS)x alloys

MANETTAS, Andrew, SANTOS, Rafael, FERRERES, Xavier Reales and AMINORROAYA YAMINI, Sima <http://orcid.org/0000-0002-2312-8272>

Published version

MANETTAS, Andrew, SANTOS, Rafael, FERRERES, Xavier Reales and AMINORROAYA YAMINI, Sima (2018). Thermoelectric performance of single phase p-type quaternary (PbTe)0.65–x(PbSe)0.35(PbS)x alloys. ACS Applied Energy Materials, 1 (5), 1898-1903.

Thermoelectric Performance of Single Phase *p*-type Quaternary $(PbTe)_{0.65-x}(PbSe)_{0.35}(PbS)_x$ Alloys

Andrew Manettas[1], Rafael Santos[1], Xavier Reales Ferreres[1], Sima Aminorroaya Yamini[1, 2]*

1. Australian Institute for Innovative Materials (AIIM), Innovation Campus, University of Wollongong, Squires Way, North Wollongong, NSW 2500, Australia
2. Department of Engineering and Mathematics, Sheffield Hallam University, Sheffield, S1 1WB, UK. Email: S.Aminorroaya@shu.ac.uk

Abstract

Recently, the quaternary system PbTe-PbSe-PbS has been shown to provide high thermoelectric efficiency, *z*T. The intent of this research is to investigate the thermoelectric properties of Na-doped pseudoternary $(PbTe)_{0.65-x}(PbSe)_{0.35}(PbS)_x$ with a high ratio of PbS to PbTe. The addition of a large concentration of PbSe increases the solubility limit of PbS in PbTe, allowing all samples to behave as solid solutions with a high concentration of PbS. This is proved to decrease lattice thermal conductivity due to the larger atomic mass contrast between Sulphur and Tellurium, however, simultaneously causes a decrease in the Seebeck coefficient due to a larger band offset, so a high concentration of PbS shows no improvement in *z*T, with a maximum of ~1.4 in the $x = 0$, 0.05 and 0.10 samples.

Keywords: p-Type; Thermal conductivity; XRD; Pb-chalcogenide; Electronic band structure

1. Introduction

Solid-state thermoelectric generators, which convert heat to electricity, have been identified as candidates for waste heat recovery[1]. The conversion efficiency is defined by the dimensionless thermoelectric figure-of-merit $zT = S^2\sigma T/\kappa$, where T is the operating temperature, S is the Seebeck coefficient, σ is the electrical conductivity, and κ is the thermal conductivity, consisting of the lattice and electronic components of the thermal conductivity, κ_L and κ_e, respectively. Alloying thermoelectric materials provides wide control of different material properties, including the thermal conductivity, structural properties, band gap, and carrier density which all contribute to the thermoelectric performance[2-3]. Among the thermoelectric materials, lead chalcogenides have been shown to have high conversion efficiencies in the mid-range temperature region (~ 300 – 600 °C)[4]. The high performance of PbTe is achieved by tuning the electronic structure near the Fermi level, manipulating and utilising the material's multiple bands, and altering the band gap[5-6].

Several studies on PbTe alloys report a high figure-of-merit for the single phase ternary PbTe-PbSe system[7-8]. Alloying PbTe with PbSe alters the convergence temperature of the light and heavy hole valence bands[9]. By having a higher convergence temperature than that of pure PbTe, the power factor is maximized at a higher temperature, resulting in a greater zT at ~ 580 °C. In the PbTe-PbS system, low thermal conductivity due to alloying, as well as nanostructuring, leads to high thermoelectric performance[10]. The reduction in thermal conductivity comes from phonon scattering at the interfaces of the secondary phases, as PbS shows very limited solubility in the PbTe matrix[11].

The PbSe-PbS system has been researched[12] and has shown to decrease lattice thermal conductivity compared to the PbSe and PbS binary systems due to impurity scattering, however in extrinsic PbSe-PbS[2] this improvement does not lead to a higher zT than the PbTe-PbSe system due to a reduced power factor from a lower carrier mobility.

The ternary PbTe–PbSe and PbSe–PbS systems have unlimited solubility over the entire composition range and as such, are always solid solutions[12-13]. Nevertheless, the components of the PbTe–PbS system show very limited solubility with respect to each other, and phase separation of PbS precipitates in the PbTe matrix on the PbTe-rich side of the phase diagram occurs via nucleation and growth. This behaviour is also observed in the quaternary system PbTe–PbSe–PbS, where the addition of PbS causes a secondary phase to appear[14]. A large amount of PbSe increases the solubility of PbS in PbTe[15], allowing $(PbTe)_{0.65-x}(PbSe)_{0.35}(PbS)_x$ samples to be still behave as solid solutions with a large concentration of PbS in the PbTe matrix. Single phase samples can maintain lower thermal conductivity, as PbS has a higher lattice thermal conductivity than PbTe, and a large volume fraction of PbS precipitates in multiphase samples results in an increase in the lattice thermal conductivity[5].

Sodium is a commonly used *p*-type dopant for lead chalcogenides,[10, 14] and in heavily doped multiphase PbTe-PbS samples a large percentage of sodium will partition to the secondary PbS phase. This sodium segregation is detrimental to performance[4], therefore, single phase sodium doped PbTe is of interest in order to maximize the power factor.

Synthesis of the quaternary PbTe-PbSe-PbS system with sodium doping enables a greater power factor, similar to that in the PbTe-PbSe system, although a decrease in the Seebeck coefficient is seen due to the increased concentration of PbS, decreasing the power factor overall. In addition to the power factor modification, a simultaneous decrease in lattice thermal conductivity, similar to that in the PbTe-PbS system, leads to an improved zT.

2. Experimental

2.1 Sample Fabrication

Pure PbS was fabricated by mixing a stoichiometric ratio of Pb (99.999%) and S (99.999%) and reacting at high temperature in an evacuated quartz ampoule, which is

followed by furnace cooling. The $Pb_{0.98}Na_{0.02}Te_{0.65-x}Se_{0.35}S_x$ (x = 0, 0.05, 0.10, 0.15, 0.20) samples were fabricated by mixing a stoichiometric ratio of high purity Pb (99.999%), Se (99.999%), PbS, Te (99.9%), and Na (99.9%) in an evacuated carbon-coated quartz ampoule and heating to 1100° C. Samples were held at that temperature for 10 hours to homogenise the melt, followed by water quenching. These samples were then annealed at 550 °C for 72 hours. The resulting ingot was then hand ground into a fine powder and sintered using spark plasma sintering (SPS) under vacuum at an axial pressure of 40 MPa, 520 °C for 30 minutes.

2.2 Transport property measurements

The thermal diffusivity (λ) was measured using a Linseis LFA 1000 instrument with the laser flash method, and the thermal conductivity (κ) was calculated by $\kappa = C_p \times \lambda \times d$. The density ($d$) was calculated using the measured weight and dimensions of the sample, and the specific heat capacity (C_p) was estimated using: $C_p\ (k_B\ per\ atom) = (3.07 + 4.7 \times 10^{-4} \times (\frac{T}{K} - 300))^8$

The resistivity (ρ) and Seebeck coefficient (S) were measured in a Linseis LSR-3. The combined uncertainty for all measurements involved in zT determination is ~20%.

2.3 Hall measurements:

The low temperature (5 – 400 K) Hall coefficient was measured using a Quantum Design Physical Properties Measurement System (PPMS-14T) up to 2T. The carrier concentration (n) is calculated from: $n = 1/eR_H$, where e is the electronic charge and R_H is the Hall coefficient.

2.4 Materials characterisation

2.4.1 X-ray diffraction

The crystallographic structure and composition were determined using X-ray diffraction

(XRD) with a GBCeMMA X-ray diffractometer with Cu Kα radiation (λ = 1.544 Å, 40 kV, 25 mA). The lattice parameters were calculated using Rietveld analysis of X-ray diffraction patterns.

2.4.2 Electron microscopy analyses

To study the microstructures of compositions x = 0.05 and x = 0.15 the samples were hot mounted in Struers Polyfast conductive resin. Samples were first mechanically polished down to a 1 μm surface roughness followed by fine polishing using cross-sectional ion milling on a Leica TIC -020 operating at 2 kV for 20 minutes.

Scanning electron microscopy (SEM) on the samples was conducted in a JEOL JSM 7001F microscope equipped with Energy Dispersive X-ray Spectroscopy (EDS). The conditions for analysis were set at 15 kV, ~5.1 nA probe current, and 10 mm working distance fitted with an Oxford Instruments Nordlys-II camera interfacing with the Aztec software suite.

3. Results/Discussion

The X-ray diffraction patterns of all the samples are shown in Figure 1(a), which can be indexed to the NaCl type face-centred cubic (FCC) crystal structure, with no evidence of a secondary phase. As there is further alloying with PbS, the diffraction peaks are shifted to higher angles, as PbS has a smaller lattice parameter (5.36 Å) than both PbTe (6.46 Å) and PbSe (6.12 Å). Rietveld refinement was utilised to accurately determine the lattice parameters of the matrix by extrapolating from high angle diffraction peaks. The lattice parameter as a function of the PbS concentration is shown in Figure 1(b). The lattice parameter decreases linearly with increasing PbS, following Vegard's law for solid solutions.

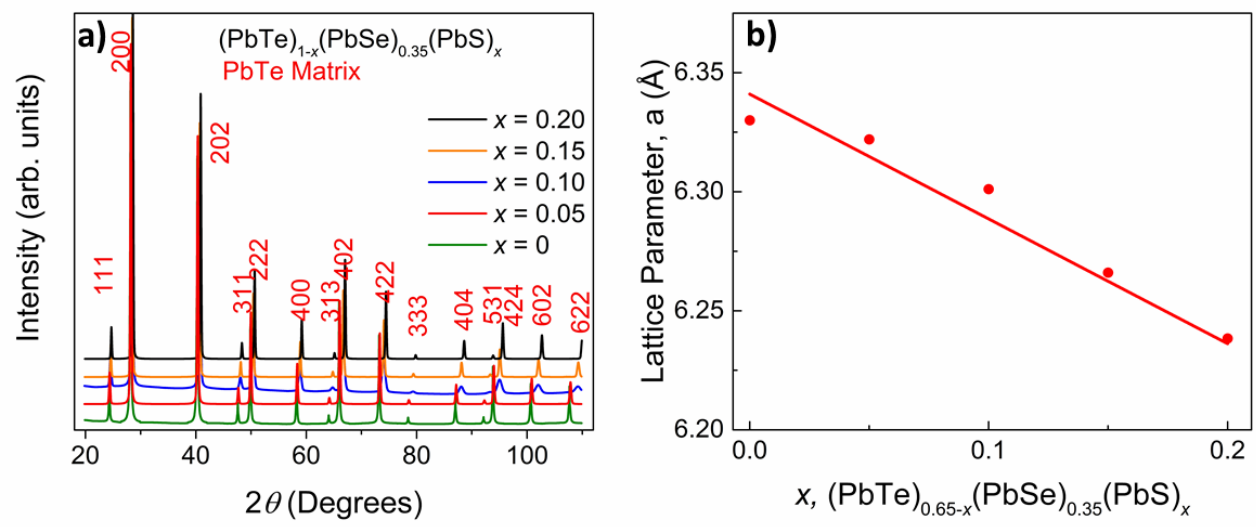

Figure 1 (a) XRD patterns of *p*-type $(PbTe)_{0.65-x}(PbSe)_{0.35}(PbS)_x$ samples (x = 0, 0.05, 0.10, 0.15, 0.20), showing diffraction peaks from the PbTe matrix. A shift of the peaks towards higher angles is seen when PbSe is added and also as the PbS content increases; (b) Lattice parameter of *p*-type $(PbTe)_{0.65-x}(PbSe)_{0.35}(PbS)_x$ samples (x = 0, 0.05, 0.10, 0.15, 0.20) as a function of PbS content.

The microstructures of samples x = 0.05 and 0.15 were studied via scanning electron microscopy (SEM) equipped with electron dispersive X-ray spectroscopy (EDS).

Micrographs in Figure 2 are representative of microstructures found in sample x = 0.05 and shows large variation in grain size comprising grains larger than 50 µm down to just a few microns. However, to the extent that SEM analysis permits no precipitates were found in the matrix. Figure 2(a) shows a magnified view of fewer grains, where grain boundaries are defined clearly without the apparent formation of precipitates. Moreover, a qualitative investigation of chemical composition was undertaken by point and area EDS analysis. These reported results of similar compositions across the grains suggesting that no secondary phases were formed and that the difference seen in grain's contrast is due to their different crystallographic orientation.

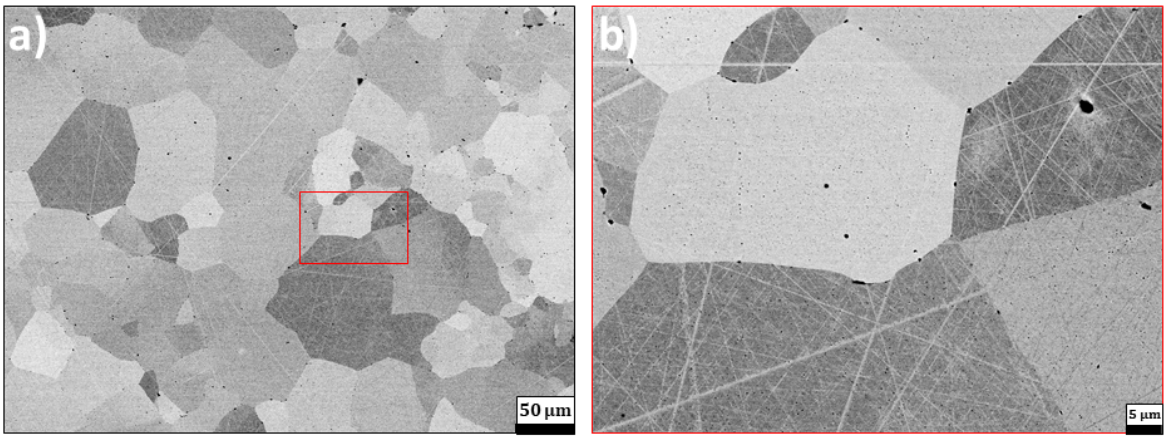

Figure 2 – (a) SEM micrograph of sample $Pb_{0.98}Na_{0.02}Te_{0.65-x}Se_{0.35}S_x$ (x = 0.05). (b) Micrograph representing marked area in solid red line in (a)

Figure 3 micrographs correspond to sample x = 0.15, these are considered characteristic of the sample, showing homogeneous porosity within the grains and grain boundaries as seen in Figure 3(a). However, qualitative chemical analysis was conducted using EDS point and area analysis revealing no signs of secondary phases or precipitates. Figure 3(b) highlights delineated grain boundaries and grain contract is due to different crystallographic orientation.

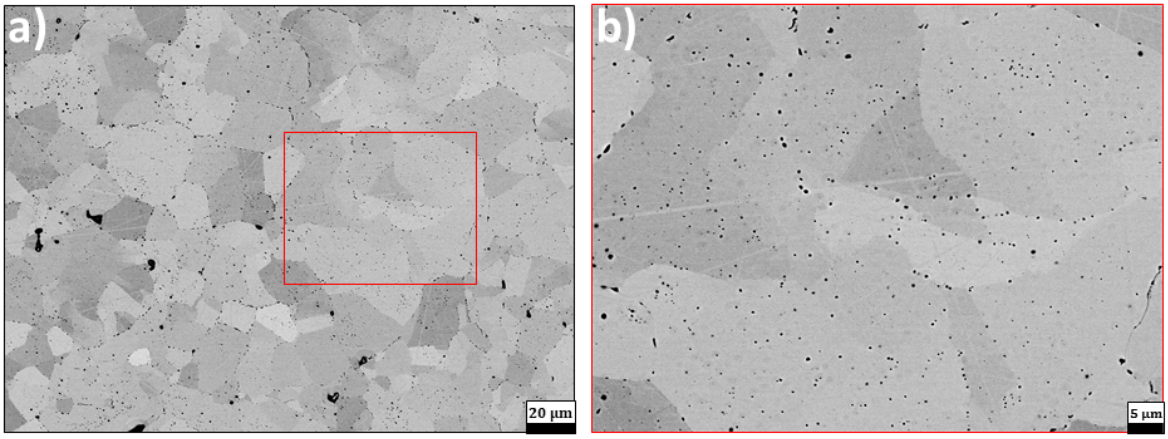

Figure 3 - (a) SEM micrograph of sample $Pb_{0.98}Na_{0.02}Te_{0.65-x}Se_{0.35}S_x$ (x = 0.15). (b) Micrograph representing marked area in solid red line in (a)

The resistivity and Seebeck coefficient of all the $(PbTe)_{0.65-x}(PbSe)_{0.35}(PbS)_x$ samples as a function of temperature are shown in Figure 4(a) and Figure 4(b), respectively. The addition of PbS does not have a significant effect on the resistivity, with the x = 0.05, 0.10, and 0.20 samples having a similarly high maximum resistivity of ~3.2 mΩ·cm at 850 K, and the x = 0

and 0.15 samples have slightly lower ones at ~3 and ~2.8 mΩ·cm, respectively. Figure 4(b) shows the Seebeck coefficients of all the samples as a function of temperature. An increase in the PbS content causes a systematic decrease in the Seebeck coefficient value at 850 K from ~ 250 μV/K for $x = 0$ to ~ 200 μV/K for $x = 0.20$. This decrease in the Seebeck coefficient can be attributed to the expected larger energy band offset between the light and heavy hole bands obtained through alloying with PbSe and PbS[16].

As the temperature rises in PbTe, the energy of the light valence band (L) is reduced until it reaches the heavy valence band (Σ) band edge[17]. The density of states (DOS) in the Σ band is much higher, and it provides a higher Seebeck coefficient than that with the L band alone, given the same carrier density. The convergence of valence bands results in higher thermoelectric efficiency at operating temperatures near 600 K in heavily doped materials where the Σ band contributes to the electronic properties of the alloy. At a given carrier concentration, a high Seebeck coefficient can be achieved due to the high DOS effective mass. A large total DOS can be due to either large band degeneracy or a high single-valley density-of-states effective mass of the degenerate valleys.

The band gap and the energy offset between the two valence bands in PbTe have been shown to be adjustable by alloying with PbSe and PbS[17-18]. Electronic band structure calculations show that the Σ-band exists at a lower energy level than PbTe in both PbSe and PbS[19], so it is expected that the heavy valence band would move to lower energy levels with PbSe and PbS alloying. This larger band offset decreases the effective mass (m^*) and consequently lowers the Seebeck coefficient. The band gap of the $(PbTe)_{0.65-x}(PbSe)_{0.35}(PbS)_x$ system increases with added PbS[15], and this causes a decrease in the contribution to electrical conduction by minority carriers[20], which are thermally excited across the band gap, delaying the maximum Seebeck coefficient value to a higher temperature.

Figure 4(a) demonstrates that the resistivity value changes almost linearly with the temperature, and Figure 4(b) shows that the Seebeck coefficient reaches the plateau region at temperatures higher than 750 K, indicating that alloying with PbSe and PbS has increased the energy band offset, with the convergence of bands occurring at much higher temperatures.

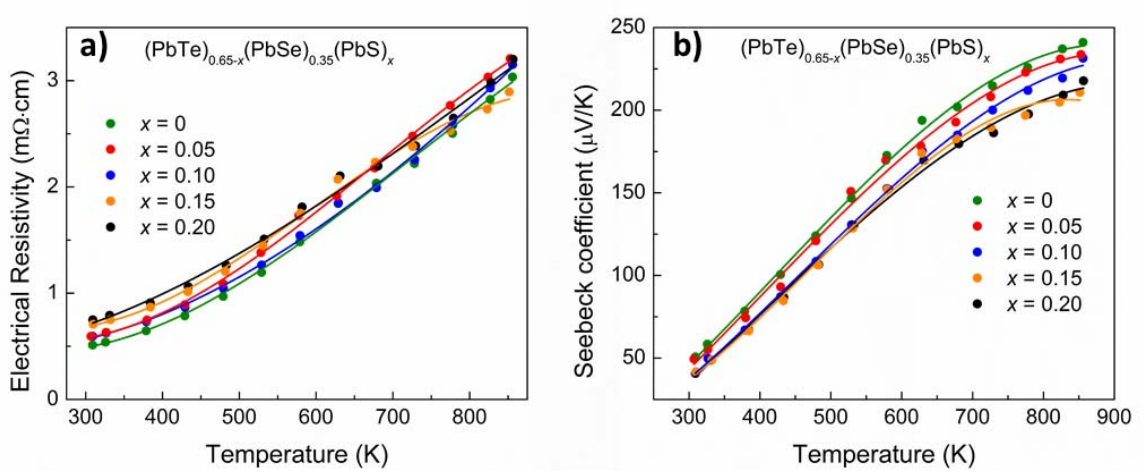

Figure 4 – Electronic transport properties of *p*-type $(PbTe)_{0.65-x}(PbSe)_{0.35}(PbS)_x$ (x = 0, 0.05, 0.10, 0.15, 0.20) samples: (a) Resistivity; (b) Seebeck coefficient for all samples, the Seebeck coefficient increases across the entire temperature range. The addition of PbS to this system decreases the Seebeck coefficient for the PbTe rich samples.

The temperature dependence curves of the Hall coefficient (R_H) of the $(PbTe)_{0.65-x}(PbSe)_{0.35}(PbS)_x$ samples (x = 0, 0.05, 0.10, 0.15, 0.20) exhibit extremely low R_H values (Figure 5), in line with the high concentration of dopant, which resulted in a charge carrier concentration, n, of approximately 1×10^{20} - 3.5×10^{20} cm^{-3}. The temperature dependence of the Hall coefficient for all the samples shows typical two-band behaviour[5]: at low temperatures, R_H is roughly constant, as the majority of the holes are located in the higher-energy-level L valence band[16-17]; at temperatures above ~100 K, a significant upturn in R_H is observed, due to an increased contribution to the electronic conduction by the Σ band, as, above this temperature, holes are able to populate both valence subbands.

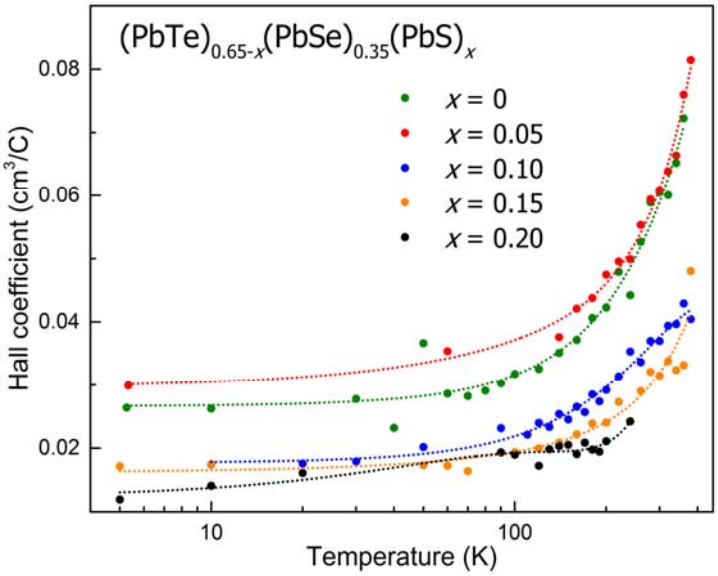

Figure 5 Hall coefficient temperature dependence of *p*-type $(PbTe)_{0.65-x}(PbSe)_{0.35}(PbS)_x$ (x = 0, 0.05, 0.10, 0.15, 0.20).

Table 1 shows that the addition of PbS (band gap, E_g = 0.37 eV) to PbSe (E_g = 0.27 eV) and PbTe (E_g = 0.29 eV) increases the band gap of the alloy[15]. An increase in band gap delays the maximum Seebeck value to a higher temperature[20], and in the PbTe-PbSe system, allows the compound to reach a higher maximum Seebeck value due to the altered band structure[7], although in the current set of samples, where the ternary system of $(PbTe)_{0.65}(PbSe)_{0.35}$ compound is alloyed with PbS, the Seebeck coefficient values are decreased by alloying at a constant Na dopant concentration (1 at.% Na). This follows from the results seen previously in Figure 4(b), where an increased band offset decreases the effective mass and leads to the decrease in the Seebeck coefficient.

Table 1 - Carrier concentrations and band gaps of *p*-type $(PbTe)_{0.65-x}(PbSe)_{0.35}(PbS)_x$ (x = 0, 0.05, 0.10, 0.15, 0.20).

Composition	Carrier concentration (cm^{-3})		Band Gap (eV) [15]
	Below 100K	Room temperature	
$x = 0$	1.7×10^{20}	1.0×10^{20}	0.305
$x = 0.05$	1.7×10^{20}	1.0×10^{20}	0.310

$x = 0.10$	2.7×10^{20}	1.7×10^{20}	0.318
$x = 0.15$	2.4×10^{20}	2.0×10^{20}	0.325
$x = 0.20$	2.5×10^{20}	4.3×10^{20}	0.335

Figure 6(a) shows the total thermal conductivity as a function of temperature for all $(PbTe)_{0.65-x}(PbSe)_{0.35}(PbS)_x$ samples. All samples show behaviour that is typical of heavily doped semiconductors, where the thermal conductivity decreases with increasing temperature. Replacing matrix atoms with larger mass-contrast atoms reduces the lattice thermal conductivity of the solid solution alloys[17]. The large mass contrast between the Sulphur atoms and the Tellurium matrix atoms is responsible for the significant reduction in the lattice thermal conductivity, which originates from phonon scattering on solute atoms of sulphur-containing alloys[17-18]. This explains the decrease in thermal conductivity with PbS alloying of $(PbTe)_{0.65}(PbSe)_{0.35}$ (Figure 6(a)). The lattice thermal conductivity (κ_L) is shown in Figure 6(b) and is calculated by $\kappa_L = \kappa - ([1.5+e^{(-S/116)}\times10^{-3}]\times T/\rho)$ [21]

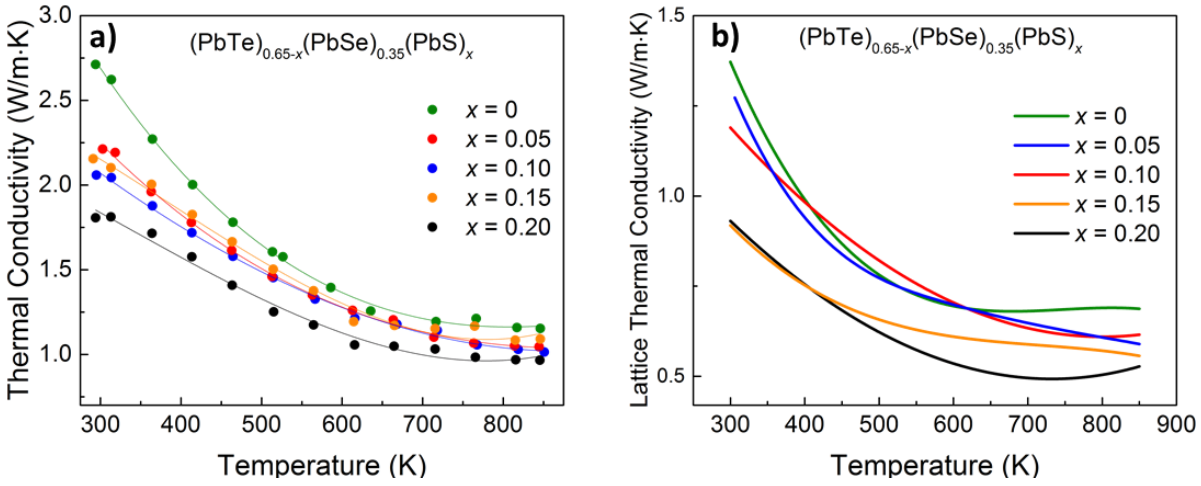

Figure 6 (a) Thermal conductivity of *p*-type $(PbTe)_{0.65-x}(PbSe)_{0.35}(PbS)_x$ samples (x = 0, 0.05, 0.10, 0.15, 0.20), with all samples showing a decrease in κ as T increases, as well as an overall decrease as the PbS content increases in the PbTe rich samples; (b) Lattice thermal conductivity of *p*-type $(PbTe)_{0.65-x}(PbSe)_{0.35}(PbS)_x$ samples (x = 0, 0.05, 0.10, 0.15, 0.20), with

all samples showing a decrease in κ_L as T increases, as well as an overall decrease as the PbS content increases in the PbTe rich samples

The room temperature Seebeck coefficient and resistivity were measured using home-built devices. The resistivity apparatus uses the van der Pauw method. The results in Table 2 show that the Seebeck coefficient decreases from ~50 μV/K to ~38 μV/K with added PbS and that there in an increase in the resistivity with additional PbS content at higher concentrations ($x = 0.15$, $x = 0.20$.) There is good agreement with the results from both the room temperature data obtained from the home-built devices (Table 2) and results obtained from the Linseis LSR (Figure 4).

Table 2 Room-temperature resistivity and Seebeck coefficient of *p*-type $(PbTe)_{0.65-x}(PbSe)_{0.35}(PbS)_x$ ($x = 0$, 0.05, 0.10, 0.15, 0.20).

Composition	Resistivity (mΩ·cm)	Seebeck coefficient (μV/K)
$x = 0$	0.59	48.34
$x = 0.05$	0.61	50.39
$x = 0.10$	0.60	38.81
$x = 0.15$	0.76	39.56
$x = 0.20$	0.75	38.31

The calculated values for zT, from the measured results, of all the samples up to 850 K are shown in Figure 7. The thermal conductivity is improved with increasing PbS content, although a simultaneous decrease in the Seebeck coefficient and increase in the resistivity occur with no overall benefit to zT. The $x = 0$, 0.05, and 0.10 compounds have the highest zT of ~1.4 at 850 K. Comparing these 35% PbSe samples to the similarly doped 10% PbSe

system[11], which has a maximum zT of ~1.5 for 5% PbS, shows that there is no significant improvement in zT by alloying the PbTe-PbSe system with a larger percentage of PbS.

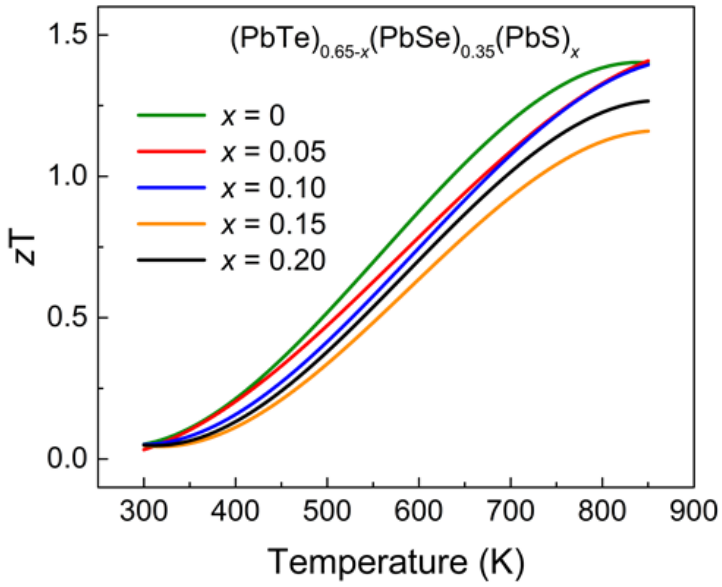

Figure 7 Figure of merit (zT) of p-type $(PbTe)_{0.65-x}(PbSe)_{0.35}(PbS)_x$ samples (x = 0, 0.05, 0.10, 0.15, 0.20), showing a maximum zT for the x = 0, 0.05, and 0.10 samples, and a decrease in thermoelectric performance with additional PbS content.

4. Conclusion

The maximum zT value for all the $(PbTe)_{0.65-x}(PbSe)_{0.35}(PbS)_x$ (x = 0, 0.05, 0.10, 0.15, 0.20) samples is ~1.4 at 850 K for three different samples (x = 0, 0.05, and 0.10). This is slightly lower than for similarly alloyed systems with 10% PbSe[11], although this is advantageous, as tellurium is a rare element and, as such, is increasing in value, so replacing it with sulphur without any significant detriment to the overall performance represents progress towards lower tellurium concentrations in thermoelectric materials.

Acknowledgements

This research has been conducted with the support of an Australian Research Council Discovery Early Career Award (DE130100310); and the Australian Government Research Training Program Scholarship.

References

(1) Dughaish, Z. Lead Telluride as a Thermoelectric Material for Thermoelectric Power Generation *Physica B: Condensed Matter* **2002**, *322*, 205-223.

(2) Wang, H.; Wang, J.; Cao, X.; Snyder, G. J. Thermoelectric Alloys Between PbSe and PbS with Effective Thermal Conductivity Reduction and High Figure of Merit *Journal of Materials Chemistry A* **2014**, *2*, 3169-3174.

(3) Yamini, S. A.; Wang, H.; Ginting, D.; Mitchell, D. R.; Dou, S. X.; Snyder, G. J. Thermoelectric Performance of n-type $(PbTe)_{0.75}(PbS)_{0.15}(PbSe)_{0.1}$ Composites *ACS applied materials & interfaces* **2014**, *6*, 11476-11483.

(4) Aminorroaya Yamini, S.; Mitchell, D. R. G.; Wang, H.; Gibbs, Z. M.; Pei, Y.; Dou, S. X.; Snyder, G. J. Origin of Resistivity Anomaly in p-type Leads Chalcogenide Multiphase Compounds *AIP Advances* **2015**, *5*, 053601-053607.
(5) Ravich, Y. I. *Monographs in Semiconductor Physics. Semiconducting Lead Chalcogenides*. ed. L.S. Stil'bans Vol.5. 1970, New York: Plenum Press 377.
(6) LaLonde, A. D.; Pei, Y.; Wang, H.; Jeffrey Snyder, G. Lead Telluride Alloy Thermoelectrics *Materials Today* **2011**, *14*, 526-532.
(7) Zhang, Q.; Cao, F.; Liu, W.; Lukas, K.; Yu, B.; Chen, S.; Opeil, C.; Broido, D.; Chen, G.; Ren, Z. Heavy Doping and Band Engineering by Potassium to Improve the Thermoelectric Figure of Merit in p-type PbTe, PbSe, and $PbTe_{(1-y)}Se_{(y)}$ *Journal of the American Chemical Society* **2012**, *134*, 10031-10038.
(8) Wang, H.; Pei, Y.; LaLonde, A. D.; Snyder, G. J. Heavily Doped p-type PbSe with High Thermoelectric Performance: an Alternative for PbTe *Advanced materials* **2011**, *23*, 1366-1370.
(9) Wang, H.; Gibbs, Z. M.; Takagiwa, Y.; Snyder, G. J. Tuning Bands of PbSe for Better Thermoelectric Efficiency *Energy Environ. Sci.* **2014**, *7*, 804-811.
(10) Jaworski, C. M.; Nielsen, M. D.; Wang, H.; Girard, S. N.; Cai, W.; Porter, W. D.; Kanatzidis, M. G.; Heremans, J. P. Valence-Band Structure of Highly Efficient p-type Thermoelectric PbTe-PbS Alloys *Physical Review B* **2013**, *87*, 045203.
(11) Aminorroaya Yamini, S.; Wang, H.; Gibbs, Z. M.; Pei, Y.; Mitchell, D. R. G.; Dou, S. X.; Snyder, G. J. Thermoelectric Performance of Tellurium-Reduced Quaternary p-type Lead–Chalcogenide Composites *Acta Materialia* **2014**, *80*, 365-372.
(12) Wang, J. L.; Wang, H.; Snyder, G. J.; Zhang, X.; Ni, Z. H.; Chen, Y. F. Characteristics of Lattice Thermal Conductivity and Carrier Mobility of Undoped PbSe-PbS Solid Solutions *Journal of Physics D: Applied Physics* **2013**, *46*, 405301.
(13) Volykhov, A. A.; Yashina, L. V.; Shtanov, V. I. Phase Equilibria in Pseudoternary Systems of IV–VI Compounds *Inorganic Materials* **2010**, *46*, 464-471.
(14) Aminorroaya Yamini, S.; Brewis, M.; Byrnes, J.; Santos, R.; Manettas, A.; Pei, Y. Z. Fabrication of Thermoelectric Materials – Thermal Stability and Repeatability of Achieved Efficiencies *J. Mater. Chem. C* **2015**, *3*, 10610-10615.
(15) Aminorroaya Yamini, S.; Patterson, V.; Santos, R. Band-Gap Nonlinearity in Lead Chalcogenide (PbQ, Q = Te, Se, S) Alloys *ACS Omega* **2017**, *2*, 3417-3423.
(16) Pei, Y.; Shi, X.; LaLonde, A.; Wang, H.; Chen, L.; Snyder, G. J. Convergence of Electronic Bands for High Performance Bulk Thermoelectrics *Nature* **2011**, *473*, 66-69.
(17) Yamini, S. A.; Wang, H.; Gibbs, Z. M.; Pei, Y.; Dou, S. X.; Snyder, G. J. Chemical Composition Tuning in Quaternary p-type Pb-Chalcogenides - A Promising Strategy for Enhanced Thermoelectric Performance *Physical chemistry chemical physics : PCCP* **2014**, *16*, 1835-1840.
(18) Korkosz, R. J.; Chasapis, T. C.; Lo, S. H.; Doak, J. W.; Kim, Y. J.; Wu, C. I.; Hatzikraniotis, E.; Hogan, T. P.; Seidman, D. N.; Wolverton, C.; Dravid, V. P.; Kanatzidis, M. G. High ZT in p-type $(PbTe)_{1-2x}(PbSe)_x(PbS)_x$ Thermoelectric Materials *Journal of the American Chemical Society* **2014**, *136*, 3225-3237.
(19) Zhang, Y.; Ke, X.; Chen, C.; Yang, J.; Kent, P. R. C. Thermodynamic Properties of PbTe, PbSe, and PbS: First-Principles Study *Physical Review B* **2009**, *80*, 024304.
(20) Pei, Y.; Wang, H.; Snyder, G. J. Band Engineering of Thermoelectric Materials *Advanced materials* **2012**, *24*, 6125-6135.
(21) Kim, H.-S.; Gibbs, Z. M.; Tang, Y.; Wang, H.; Snyder, G. J. Characterization of Lorenz number with Seebeck Coefficient Measurement *APL Materials* **2015**, *3*, 041506